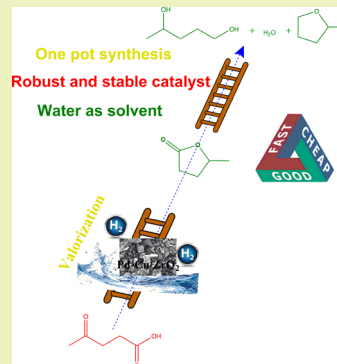


Cascade Engineered Synthesis of γ -Valerolactone, 1,4-Pentanediol, and 2-Methyltetrahydrofuran from Levulinic Acid Using Pd–Cu/ZrO₂Catalyst in Water as Solvent

Saurabh C. Patankar and Ganapati D. Yadav*

Department of Chemical Engineering, Institute of Chemical Technology, Matunga, Mumbai 400019, India

ABSTRACT: Synthesis of chemicals derived from biomass using heterogeneous catalysts with water as a solvent elegantly fits into the realm of sustainable chemistry. In this work, a novel heterogeneous palladium copper bimetallic catalyst supported on zirconia was synthesized and fully characterized. This catalyst was used in one-pot synthesis of γ -valerolactone, 1,4-pentanediol, and 2-methyl tetrahydrofuran from levulinic acid and hydrogen using water as a solvent. The catalyst consists of 1% palladium and 29% copper supported on zirconia and is characterized per se and after reuse by using elemental analysis, FTIR, NH₃-TPD, XRD, and BET surface area, XPS, SEM, and TEM analysis. This is the first ever report on the direct synthesis of 1,4-pentanediol and 2-methyl tetrahydrofuran using water as a solvent. Reaction mechanism and kinetic modeling was done to validate the experimental results. The results reported are thus a combination of synthesis of a novel catalyst with its full characterization, its application in a novel synthesis route, description of the synthesis mechanism and kinetic modeling, and proof of the robustness of the developed catalyst by reusing it for four catalytic cycles.



KEYWORDS: Cascade engineering, One-pot synthesis, Biomass conversion, γ -Valerolactone, 1,4-Pentanediol, 2-Methyl tetrahydrofuran, Levulinic acid, Palladium, Copper, Zirconia, Kinetics

INTRODUCTION

Developing strategies for synthesis of second-generation biofuels is a current trend. The technologies developed ought to be inexpensive and sustainable in order that both the developing countries and developed countries could adopt them. Valorization of levulinic acid (LA) derived from renewable sources; for instance, glucose and fructose, is a viable option because the products derived from it are in tune with the current liquid fuel infrastructure.¹ BioMetics Inc. developed the biorefining process to produce LA at 50–70% yields from cellulosic feed stock and estimated a large scale plant (1000–2000 ton/day) could produce LA for \$ 0.09–0.11 per kg.² There are abundant technologies for valorization of LA to γ -valerolactone (GVL) (Table 1).^{3–12} Most of these technologies employ external hydrogen as a source for hydrogenation with a suitable catalyst. Ruthenium complexes bearing monodendate phosphorus ligands are the mainly used homogeneous catalysts whereas Ru, Pd, Pt, Ni, Rh, Ir, and Au supported on neutral supports like silica or metal oxides have been used as heterogeneous catalysts.¹³ There are a very few reports on the synthesis of GVL from LA using heterogeneous non-noble catalysts. Cu/ZrO₂ and Cu/Al₂O₃ made by coprecipitation have been reported for hydrogenation of LA and methyl levulinate to GVL.⁹ Methanol and water were used as solvents. The Cu/ZrO₂ catalyst gave 100% selectivity toward GVL. However, a copper carboxylate complex was formed that resulted in leaching of the copper catalyst when water was used as a solvent. Another route to achieve formation of GVL from LA is by transfer hydrogenation. Formic acid and LA mixture in

1:1 proportion has been used with Cu/ZrO₂ catalyst prepared by oxalate gel precipitation for selective synthesis of GVL.¹⁴ Direct synthesis of 1,4-pentanediol (PDO) with 70% yield was achieved using Mo modified Rh/SiO₂ catalyst.¹⁵ The catalyst was made by incipient wetness technique and the noble metal content was 4%. Although the yield of PDO is 70%, a very high catalyst loading was used for synthesis. GVL can be further valorized to 5-nonenone in a single reactor by using a dual catalyst bed of Pd–Nb₂O₅ and ceria-zirconia.¹⁶ GVL can be hydrogenated to valeric acids and then converted to alkyl valerate esters by esterification using Pt/H-ZSM/SiO₂ catalyst.¹⁷ Decarboxylation of GVL can occur at elevated pressures over silica/alumina catalyst to produce equimolar quantities of butane and carbon dioxide. This stream is fed directly to an oligomerization reactor with H-ZSM-5 and Amberlyst A70 catalyst wherein coupling of butane monomers occurs to form condensable alkenes.¹⁸ GVL valorization has been reported to PDO and 2-methyltetrahydrofuran (2-MTHF) using 30% Cu/ZrO₂ catalyst made by oxalate gel precipitation.¹⁹ The processes for GVL valorization either use costly catalyst or severe reaction conditions.²⁰

With the objective of developing a cheap and sustainable technology for value added chemicals, we have studied systematically the synthesis of GVL, 1,4-pentanediol (PDO), and 2-methyltetrahydrofuran (2-MTHF) directly from LA.

Received: March 2, 2015

Revised: September 19, 2015

Published: September 25, 2015

Table 1. Various Technologies for Synthesis of GVL from LA

#	catalyst	reaction conditions	conversion (%)	selectivity (%)	reference
1	Ruthenium acetyl acetone	200 °C, 1200 psi H ₂ , 6 h in high pressure NMR tube	100	37	3
2	Raney Nickel	220 °C, 700 psi H ₂ , 3 h in 500 mL steel rocking bomb	100	94	4
3	5% Ru/SiO ₂	200 °C, 1400 psi with H ₂ equivalence 3.0, supercritical CO ₂ as solvent	100	100	5
4	5% Ru/C	130 °C, 170 psi H ₂ , 3 h in 1 L autoclave, 1,4-dioxane as solvent	92	99	6
5	5% Ru/C	265 °C, 14 psi H ₂ , 50 h in fixed bed, 1,4-dioxane as solvent	100	99	7
6	5% Ru/C and Amberlyst A70 as cocatalyst	70 °C, 420 psi H ₂ , 3 h in 300 mL autoclave, water as solvent	100	100	8
7	Cu/ZrO ₂ (1:1)	200 °C, 500 psi H ₂ , 5 h in 300 mL autoclave, methanol as solvent	100	90	9
8	Cu/Al ₂ O ₃ (1:1)	200 °C, 500 psi H ₂ , 5 h in 300 mL autoclave, methanol as solvent	100	86	9
9	10%Ni–7% MoO _x /C	140 °C, 120 psi H ₂ , 5 h in glass tube, no solvent	100	97	10
10	9.93% CuB ₂₃ /graphene	140 °C, 600 psi H ₂ , 4 h, <i>n</i> -dodecane as solvent	100	99	11
11	Cu/Cr (2:1)	200 °C, 1000 psi, 10 h in microautoclave, water as solvent	100	91	12

The work reports the synthesis of a novel and robust palladium and copper supported on zirconia (Pd–Cu/ZrO₂) catalyst for one-pot synthesis of GVL, PDO, and 2-MTHF from LA using Pd–Cu/ZrO₂ catalyst with water as solvent. The same catalyst was used for multiple reactions in a single pot without separation and purification of intermediates and reaction of the intermediate in another reactor. Manipulation of the strength and number of particular catalytic sites has the greatest effect on product distribution and selectivity. Hence the synthesis is termed as cascade engineered synthesis.²¹ The significance of zirconia as a support vis-a-vis others such as hydrotalcite (HT), γ -alumina (Al₂O₃), and hexagonal mesoporous silica (HMS) have been highlighted. The reaction mechanism and kinetics are also presented in this work.

EXPERIMENTAL SECTION

Materials. LA (C₅H₈O₃) and pure samples of GVL (C₅H₈O₂), PDO (C₅H₁₂O₂), and 2-MTHF (C₅H₁₀O) were procured from Thermo Fischer Scientific (India) Pvt. Ltd., Mumbai. Copper(II) nitrate trihydrate (Cu(NO₃)₂·3H₂O), zirconyl nitrate (Zr(NO₃)₂ (aq), and oxalic acid ((COOH)₂·2H₂O) were procured from Thomas Baker (Chemicals) Pvt. Ltd. Palladium(II) nitrate dihydrate (Pd(NO₃)₂·2H₂O) was procured from Himedia Laboratories, Mumbai. Magnesium nitrate dihydrate (Mg(NO₃)₂·2H₂O), aluminum nitrate trihydrate (Al(NO₃)₃·3H₂O), hexadecyl amine (C₁₆H₃₅N), ethanol (C₂H₅OH), and methanol (CH₃OH) were procured from SD Fine Chem Pvt. Ltd., Mumbai. Tetraethyl orthosilicate (SiC₈H₂₀O₄) was procured from M/S Merck Chemicals India Pvt. Ltd., Mumbai.

Catalyst Synthesis. The synthesis of tunable copper supported on zirconia catalyst is reported.¹⁹ However, the copper based catalyst cannot be used directly when water is used as a solvent, as copper leaches out in the reaction medium. Hence a novel catalyst has been developed wherein the bimetallic alloy of copper with palladium prevents leaching of copper in reaction medium.

The required amounts of copper(II) nitrate trihydrate, palladium(II) nitrate dihydrate, and zirconyl nitrate were mixed in ethanol such that the concentration of the nitrate solution was 0.1 M. The total metal loading was 30% (w/w) with 1% (w/w) of palladium and 29% (w/w) copper. 20% Molar excess of oxalic acid in ethanol was added rapidly to the nitrate solution to get precipitated copper oxalate, palladium oxalate, and zirconyl oxalate. The slurry was stirred for 30 min and the precipitate separated by centrifugation. The precipitate was then calcined at 400 °C for 3 h in air. The material obtained was used as the catalyst after *in situ* reduction and was designated Pd–Cu/ZrO₂.²² For synthesizing a catalyst with 2 g of zirconia support, 3.75 g of zirconyl nitrate, 2.21 g of copper(II) nitrate trihydrate, and 50 mg of palladium nitrate dihydrate were used. The pH of the nitrate solution was 2. It has been reported earlier that complete precipitation of nitrate to oxalate occurs between pH 2 and 4.²³

HMS and Al₂O₃ were prepared by the respective known techniques.^{24,25} Hexadecylamine was used as a precursor for synthesizing HMS. Palladium(II) nitrate dihydrate and copper(II) nitrate trihydrate were dissolved in methanol and loaded by wet impregnation technique on these supports. The metal loading was similar to that used for Pd–Cu/ZrO₂ catalyst. The final catalysts were designated as Pd–Cu/HMS and Pd–Cu/Al₂O₃, respectively.

Palladium and copper were loaded on hydrotalcite using a combustion synthesis technique, because it was found to be more robust than coprecipitation, as determined earlier by our research group.²⁶ Required amounts of magnesium nitrate hexahydrate and aluminium nitrate nonahydrate were dissolved in water such that the molar ratio of Mg/Al was 2. Palladium(II) nitrate dihydrate and copper(II) nitrate trihydrate were then added to this solution. Glycerol was used as a fuel. The solution was stirred at 80 °C for 30 min and then kept in preheated muffle furnace at 500 °C and allowed to combust. The material formed post combustion was used as catalyst.

Catalyst Characterization. Temperature-programmed desorption (TPD) and temperature-programmed reduction (TPR) were used for the quantification of the acid sites and metal site strengths (Autochem II 2910, Micromeritics, USA). For TPD measurements, 20 mg of catalyst sample was placed in a quartz tube and degassed at 300 °C under flow of nitrogen. 10% (w/w) ammonia in helium was allowed to adsorb on the catalyst surface. Physisorbed gas was removed by passing inert nitrogen over the catalyst. The chemisorbed gas was desorbed using a temperature program and measured using thermal conductivity detection (TCD). For TPR measurements, 10% (w/w) hydrogen in argon was used as a probe molecule with a similar procedure as used for TPD measurements. Powder X-ray diffraction (XRD) was used for studying the crystallinity of the catalyst (Bruker D8 Advance, USA). Cu K α radiations with a beam current of 40 kV and 100 mA were used. The data were collected from 2 θ values of 2 to 80°. Fourier transformed infrared spectrum (FTIR) was obtained from the catalyst sample pressed in a KBr pellet. The spectrum was recorded with a resolution of 2 cm⁻¹ between wavenumbers of 4000 and 400 cm⁻¹. The surface properties of the catalyst were studied by the Brunauer–Emmett–Teller (BET) method (ASAP 2020, Micromeritics, USA). 200 mg of catalyst sample was degassed under vacuum at 400 °C for 4 h. Nitrogen gas was used as an adsorbent. The measurements were done at liquid nitrogen temperature using a multipoint method. Scanning electron microscopy (SEM) and energy dispersive X-ray spectroscopy (EDXS) were used to study the surface morphology and elemental composition of the catalyst (JEOL, Japan). Thermogravimetric analysis was done to check the thermal stability of the catalysts (STA 6000 Pyris). The thermal stability was studied up to 400 °C. Atomic absorption spectroscopy was used to determine quantitative leaching of copper (Lab India Analytical AA 8000). Copper was detected at a wavelength of 324.75 nm. A calibration plot was made for 1 to 5 ppm copper content. The limit of detection (LOD) for the instrument was 0.5 ppm. The leaching of palladium was detected using a PerkinElmer Optima 8000 inductively coupled plasma optical emission spectrophotometry (ICP-OES) instrument with a

CCD array detector. The detection limit for palladium was 0.002 ppm. XPS spectra of the catalyst samples were recorded on an ESCA-3 Mark II spectrometer (VG Scientific Ltd. England) using Al K α radiation (1486.74 eV). For XPS analysis, pellets of 8 mm were made from powdered samples and placed in ultra high vacuum (UHV) chamber at 10^{-9} Torr housing the analyzer. Prior to the sample being mounted in the analyzing chamber, it was kept in the preparation chamber at 10^{-9} Torr for 5 h in order to desorb any volatile species present on the catalyst.

Reaction Setup and Analysis. The experiments of hydrogenation of LA using Pd–Cu/ZrO₂ as catalyst and water as a solvent were carried out in a 100 mL batch reactor (Amar Equipments, Mumbai). The reactor was equipped with a temperature controller (± 1 °C), pressure indicator and speed controller (± 5 rpm). LA was dissolved in water and charged into the reactor along with the catalyst. The reactor was purged with nitrogen to remove traces of air and then pressurized with hydrogen. The reactor was then heated to desired temperature. In a standard reaction, 0.03 mol LA dissolved in 50 mL of water with catalyst loading of 0.2 g/cm³ was used. Periodic samples were withdrawn during the reaction. The analysis of samples was performed on GC equipped with Zebron wax plus capillary column (30 m \times 0.25 mm \times 0.25 μ m) and flame ionization detection (FID). Dimethylformamide was used as an external standard after calibration.

RESULTS AND DISCUSSION

Catalyst Characterization. The acidity of various catalysts is shown in Table 2. Pd–Cu/HT and Pd–Cu/Al₂O₃ possess

Table 2. Temperature Programmed Desorption Study Using NH₃ as Probe Molecule for Various Synthesized Catalysts for LA Hydrogenation

catalyst	mmol of ammonia chemisorbed per gram of catalyst under STP conditions (mmol NH ₃ /g _{cat})
ZrO ₂	0.17
Pd/ZrO ₂	0.17
Cu/ZrO ₂	0.50
Pd–Cu/ZrO ₂	0.37
Pd–Cu/HT	0.16
Pd–Cu/Al ₂ O ₃	0.15
Pd–Cu/HMS	0.06

weak acid sites as NH₃ is eluted in the temperature range of 120 to 200 °C. Cu/ZrO₂ and Pd–Cu/ZrO₂ possess both weak and strong acid sites as NH₃ is eluted in the temperature ranges of 120 to 200 °C and 300 to 450 °C.¹⁶ The loading of palladium on zirconia in the case of Pd/ZrO₂ was 1% (w/w), and hence it did not affect its acidity. However, when copper content was increased to 30% (w/w) on zirconia, the total acidity increased because of copper that was in oxide form. From the EDXS analysis (Table 4), it is evident that copper is loaded both within pores and on the surface of zirconia. The bimetallic loading of palladium 1% (w/w) and copper 29% (w/w) resulted in reduction in the acidity. The reason for the decrease in the acid strength of Cu/ZrO₂ after Pd loading can be due to the reduced access to the acid sites on Cu/ZrO₂ due to loading of palladium in the pores. Pd–Cu/HMS had the minimal acidity. However, it was able to catalyze the dehydration of hydroxypentanoic acid to yield GVL. The TPR analysis for the Pd–Cu/ZrO₂ catalyst (Figure 1) indicated presence of metal sites on the catalyst as 0.96 mmol/g_{cat} H₂ adsorbed on the catalyst up to 400 °C. The FTIR spectra of the Cu/ZrO₂ and Pd–Cu/ZrO₂ indicate the Cu–O vibration at 517 cm⁻¹ and hydroxyl bands bonded to tetragonal zirconia at 3368 cm⁻¹, as shown in Figure 2. The intense peaks around 1111 and 1567

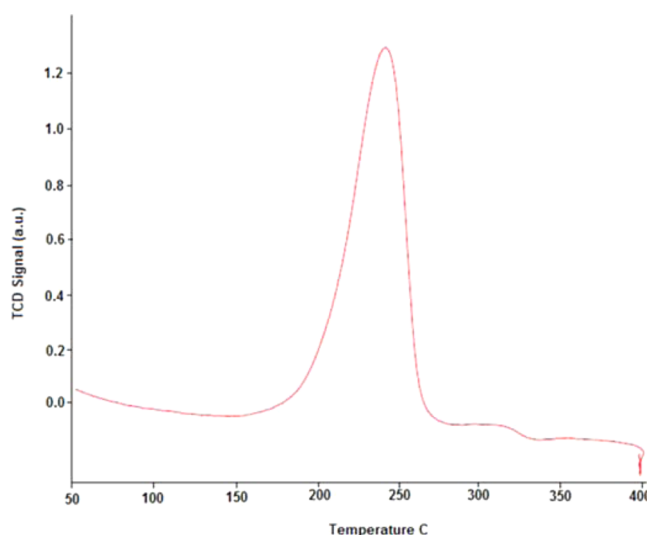


Figure 1. TPR pattern of Pd–Cu/ZrO₂ catalyst.

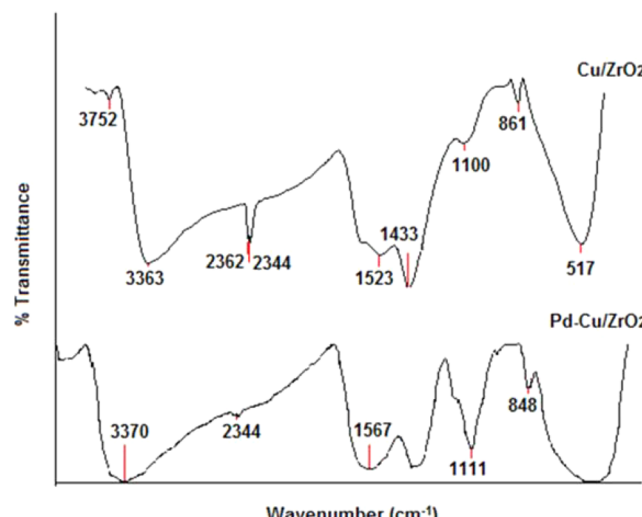


Figure 2. FTIR spectrum of Cu/ZrO₂ and Pd–Cu/ZrO₂ catalysts.

cm⁻¹ are attributed to the Pd–Cu bimetallic composite. The XRD patterns in Figure 3 for Cu/ZrO₂, Pd–Cu/ZrO₂, and used Pd–Cu/ZrO₂ catalysts indicate the presence of tetragonal zirconia at 2θ of 30.5°. The CuO phase is seen at 2θ of 35 and 39°. The PdO phase is seen at 34.5°. The reused catalyst has Cu at 43 and 70° whereas Pd is seen at around 38°.^{27–29} The in situ reduction of catalyst occurs at the start of reaction. The CuO phase is observed prior to the reaction whereas Cu and Cu₂O phases are seen postreaction. The Cu₂O phase at 50° is intact in fresh and used catalyst, indicating that it has no role in catalyzing the reaction. The XRD pattern for fresh and used Pd–Cu/HT catalyst is shown in Figure 4. The characteristic HT peaks are observed at 10° whereas the characteristic CuO peak is seen at 35°. Because the Pd–Cu/HT catalyst is amorphous, sharp peaks are not observed.

Although the loading of palladium 1% (w/w) did not reduce the acidity of zirconia, it resulted in blocking of its pores and hence increased the average pore size in Pd/ZrO₂. The surface area was also substantially reduced in Pd/ZrO₂ as compared to ZrO₂ (Table 3). When 30% (w/w) copper was loaded on zirconia, it was loaded on the surface of zirconia. It is evident from the EDXS results (Table 4). The analysis of multiple

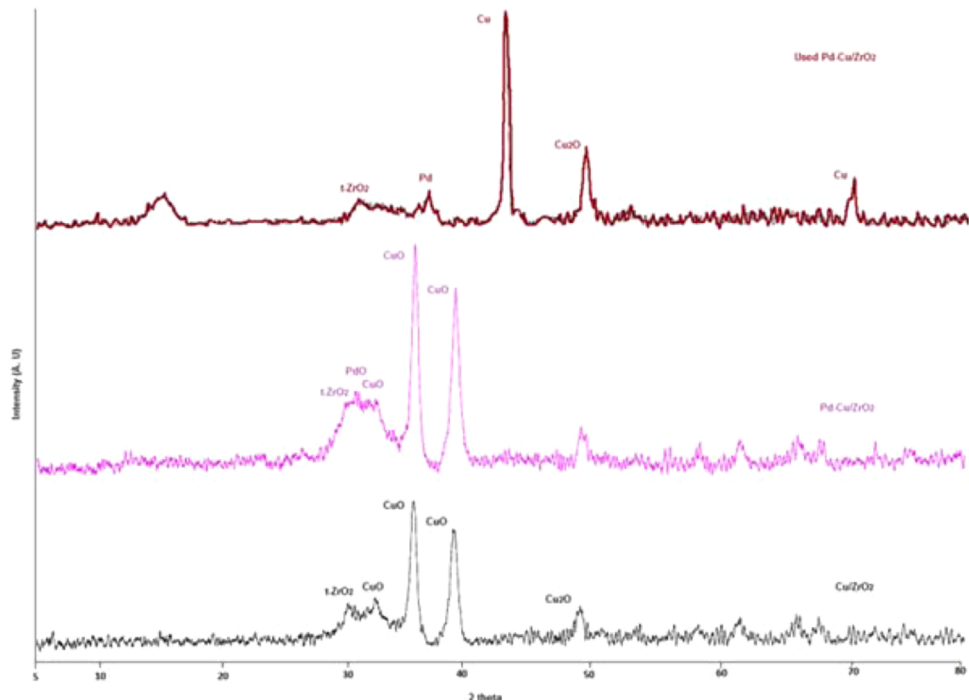


Figure 3. XRD pattern of Cu/ZrO₂, Pd–Cu/ZrO₂, and used Pd–Cu/ZrO₂ catalysts.

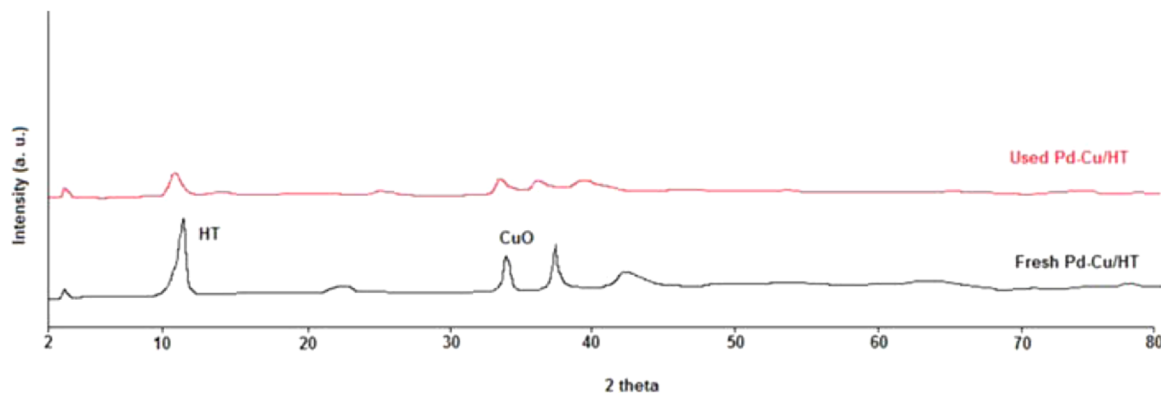


Figure 4. XRD pattern of Pd–Cu/HT and used Pd–Cu/HT catalysts.

Table 3. Surface Properties of Various Synthesized Catalysts for LA Hydrogenation

catalyst	textural property		
	surface area (m ² /g)	pore size (nm)	pore volume (cm ³ /g)
ZrO ₂	62	8	0.12
Pd/ZrO ₂	53	9	0.12
Cu/ZrO ₂	63	13	0.19
Pd–Cu/ZrO ₂	40	19	0.18
used Pd–Cu/ZrO ₂	27	27	0.16
HT	212	15	0.32
Pd–Cu/HT	188	10	0.23
Al ₂ O ₃	217	3	0.019
Pd–Cu/Al ₂ O ₃	142	4	0.06
HMS	585	4	0.65
Pd–Cu/HMS	341	5	0.32

points on the surface of Pd/ZrO₂ catalyst showed the presence of zirconium and oxygen elements whereas the analysis of multiple points on the surface of the Cu/ZrO₂ and Pd–Cu/

Table 4. Elemental Analysis of Various Synthesized Catalysts for LA Hydrogenation

catalyst	elemental analysis	
	element	mass %
Pd/ZrO ₂	Zr	74.03
	Pd	0.56
	O	25.41
	Cu	0.69
Cu/ZrO ₂	Zr	79.15
	Cu	20.17
	O	0.92
	Pd	1.74
Pd–Cu/ZrO ₂	Zr	77.29
	Cu	20.04
	O	0.92
	Pd	1.74

ZrO₂ catalyst showed the presence of copper in large proportion indicating the loading of Pd–Cu phase on zirconia. The loading of palladium blocked the pores of zirconia and hence resulted in reduced surface area of Pd–Cu/ZrO₂.

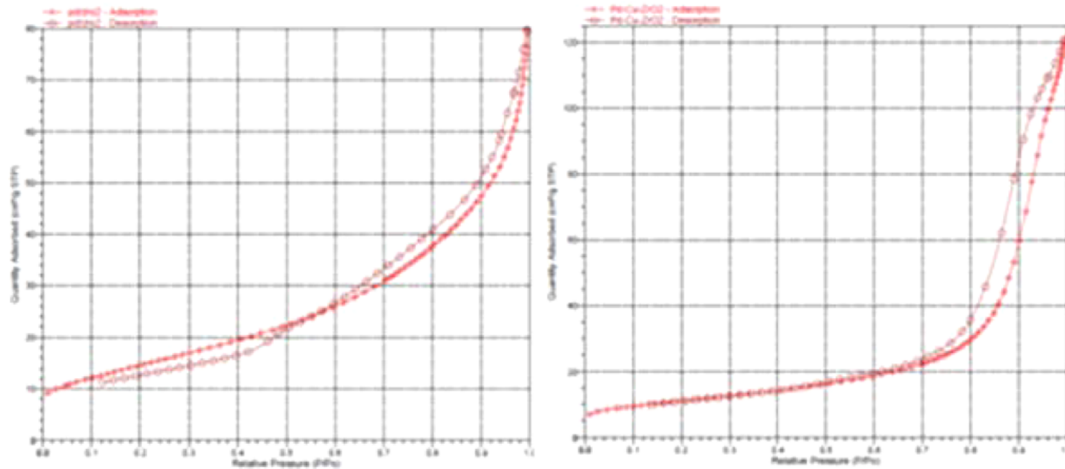


Figure 5. Adsorption desorption isotherm for Pd/ZrO_2 and $\text{Pd}-\text{Cu}/\text{ZrO}_2$ catalysts.

compared to Cu/ZrO_2 . The pore volume of $\text{Pd}-\text{Cu}/\text{ZrO}_2$ was higher as compared to $\text{Pd}-\text{ZrO}_2$ due to interconnections in pores of copper oxide coating. This is evident from Figure 5, which shows the hysteresis loop for Pd/ZrO_2 and $\text{Pd}-\text{Cu}/\text{ZrO}_2$. Pd/ZrO_2 was amorphous whereas $\text{Pd}-\text{Cu}/\text{ZrO}_2$ had a distinct morphology with sharp edges of particles (Figure 6).

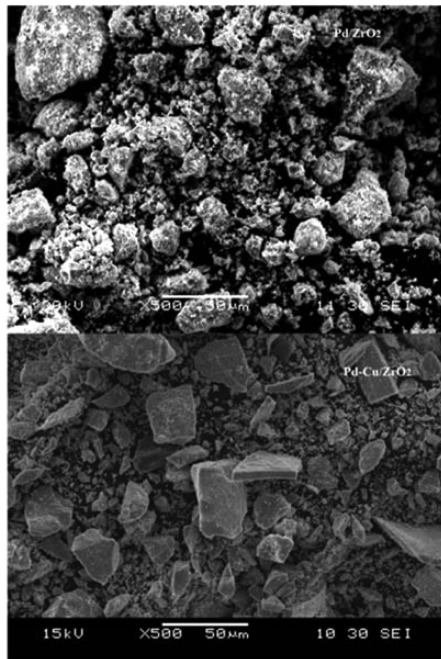


Figure 6. SEM image of Pd/ZrO_2 and $\text{Pd}-\text{Cu}/\text{ZrO}_2$ catalysts.

The loading of copper on the surface of zirconia is attributed to the oxalate gel precipitation technique in which zirconyl oxalate, copper oxalate, and palladium oxalate are formed simultaneously. In the case of $\text{Pd}-\text{Cu}/\text{HT}$ made by the combustion synthesis technique, the order in which the solid oxides are formed in the aqueous solution in the following order: palladium oxide, copper oxide, magnesium oxide, and aluminum oxide, and hence palladium and copper get loaded inside the porous matrix of HT. It is because nitrates of transition metals exhibit lower decomposition temperature than nitrates of base metal.³⁰ The back-donation of electronic cloud from nitrate to an unfilled d-orbital of transition metals results

in lower decomposition temperature in the case of palladium and copper nitrates rather than magnesium and aluminum nitrate.³¹ The pore volume of $\text{Pd}-\text{Cu}/\text{HT}$ is high because there are interconnections formed at the end due to escape of gases during combustion synthesis. In the case of $\text{Pd}-\text{Cu}/\text{Al}_2\text{O}_3$ and $\text{Pd}-\text{Cu}/\text{HMS}$, palladium and copper are loaded by a wet impregnation technique. The pore volume of $\text{Pd}-\text{Cu}/\text{Al}_2\text{O}_3$ is significantly less than other catalysts due to lack of interconnections in the pores (Figure 7). The TGA analysis showed better thermal stability of $\text{Pd}-\text{Cu}/\text{ZrO}_2$ catalyst as compared to Cu/ZrO_2 (Figure 8).^{32,33} The TEM image of $\text{Pd}-\text{Cu}/\text{ZrO}_2$ shows a specific geometry and larger particle size as compared to Cu/ZrO_2 (Figure 9) and hence has better thermal stability. The TEM image of used $\text{Pd}-\text{Cu}/\text{ZrO}_2$ catalyst is shown in Figure 10. No characteristic change in the morphology of used $\text{Pd}-\text{Cu}/\text{ZrO}_2$ catalyst is evident.

The alloy formation of $\text{Pd}-\text{Cu}$ is noticeable from the comparison of Pd 3d and Cu 2p XPS data of 1% Pd/ZrO_2 , 0.5% $\text{Pd}-29.5\%$ Cu/ZrO_2 , and 1% $\text{Pd}-29\%$ Cu/ZrO_2 catalysts (Figure 11 and Figure 12). It has been reported earlier that in the case of minimal loading of palladium with copper, an alloy is formed. The formation of alloy is evident from the shift (increase) in binding energy of palladium and copper and Cu 2p and Pd 3d peaks are visible.³⁴ It has been proved earlier that minimal loading of palladium can enhance stability of copper catalyst. Ultrasmall clusters of $\text{Pd}-\text{Cu}$ are formed such that tiny islands of palladium are present between copper clusters.³⁵

Catalytic Activity. The various supported $\text{Pd}-\text{Cu}$ synthesized catalysts were then tested for one-pot synthesis of 1,4-pentanediol and 2-methyltetrahydrofuran using water as a solvent (Table 5). Pd/ZrO_2 did not show any catalytic activity owing to small loading of palladium. Cu/ZrO_2 and $\text{Pd}-\text{Cu}/\text{ZrO}_2$ were able to catalyze the two hydrogenation and dehydration cycles to form 1,4-pentanediol and 2-methyltetrahydrofuran. In the case of Cu/ZrO_2 , the conversion was 100% after 24 h. However, there was a bluish coloration of the reaction mass, which on analysis showed 31 ppm copper suggesting leaching (Table 6). On the contrary, loading 1% Pd on Cu/ZrO_2 decreased the initial activity from 0.18 to 0.13 $\text{mol}\cdot\text{cm}^{-3}\cdot\text{min}^{-1}$ but increased the stability because no coloration was observed postreaction. ICP analysis was done to detect any leaching of palladium. It was found that after 24 h of reaction, the leaching of palladium was 0.08 ppm, which is negligible. Thus, it was clear that Pd formed an alloy with Cu

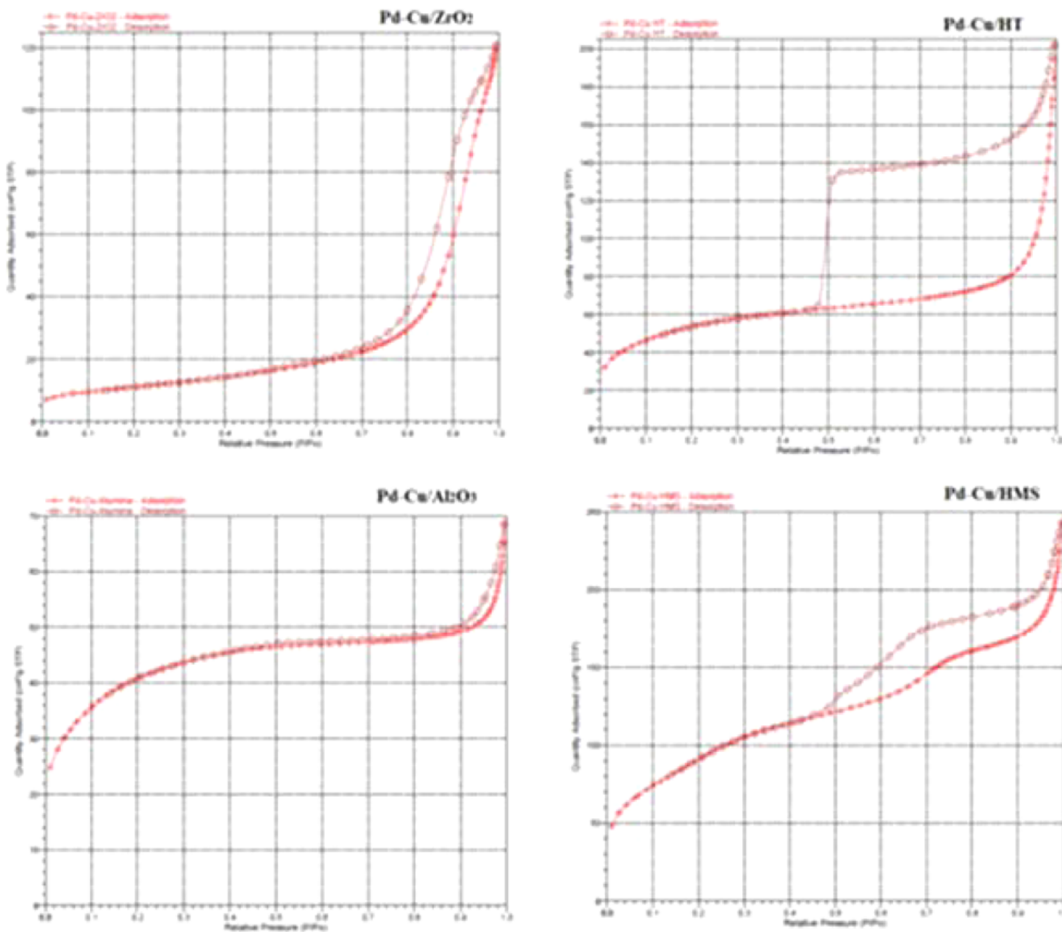


Figure 7. N_2 adsorption–desorption isotherm for Pd–Cu/ZrO_2 , Pd–Cu/HT , $\text{Pd–Cu/Al}_2\text{O}_3$, and Pd–Cu/HMS catalysts.

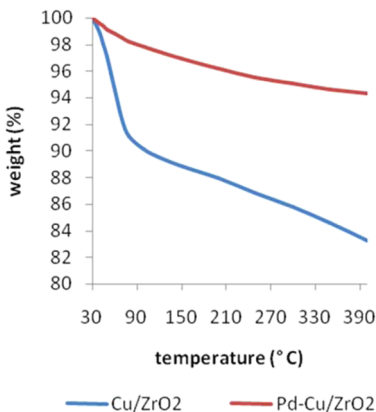


Figure 8. Thermogravimetric (TGA) analysis profile for Cu/ZrO_2 and Pd–Cu/ZrO_2 catalysts.

and prevented leaching. This is also supported by XRD patterns (**Figure 3**). The effect of other supports was studied using Pd–Cu/HT , $\text{Pd–Cu/Al}_2\text{O}_3$, and Pd–Cu/HMS , which were able to give GVL with 100% selectivity and the rates of subsequent reactions were sluggish (**Figure 13**).

The sequential reactions to yield 2-MTHF from LA are listed in **Scheme 1**. LA undergoes hydrogenation to form hydroxypentanoic acid (HPA) (reaction a). HPA undergoes dehydration to form GVL and water (reaction b). GVL undergoes hydrogenation to form PDO (reaction c) and PDO undergoes dehydration to form 2-MTHF (reaction d).

The catalytic steps involved in the one-pot synthesis of GVL, PDO, and 2-MTHF from LA using Pd–Cu/ZrO_2 catalyst and water as a solvent are

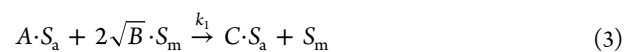
(1) Adsorption of hydrogen on metal site:



(2) Adsorption of LA on acid site:



(3) Hydrogenation of LA on to form HPA:



(4) Dehydration of HPA to form GVL:



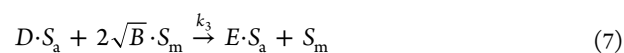
(5) Desorption of GVL from acid site:



(6) Readsorption of GVL on acid site:



(7) Hydrogenation of GVL to form PDO:



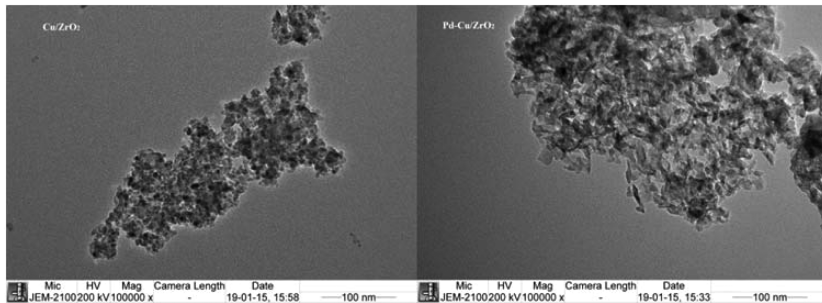


Figure 9. TEM image of Cu/ZrO₂ and Pd–Cu/ZrO₂ catalyst.

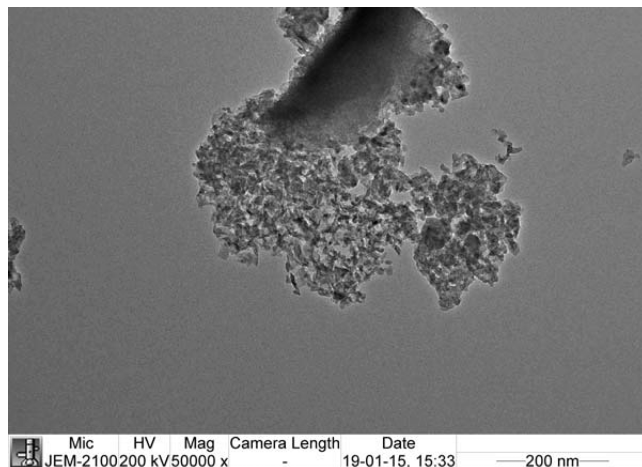


Figure 10. TEM image of used Pd–Cu/ZrO₂ catalyst.

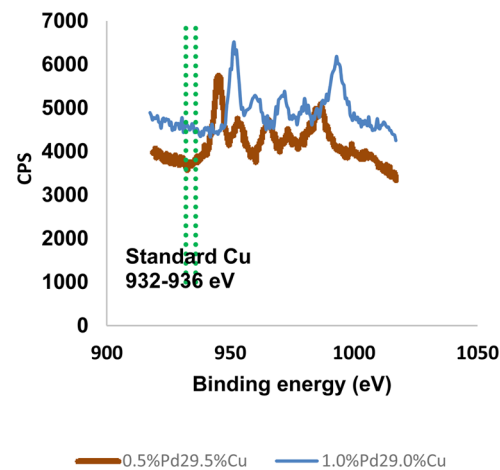


Figure 12. Cu 2p XPS of Pd–Cu/ZrO₂ catalyst.

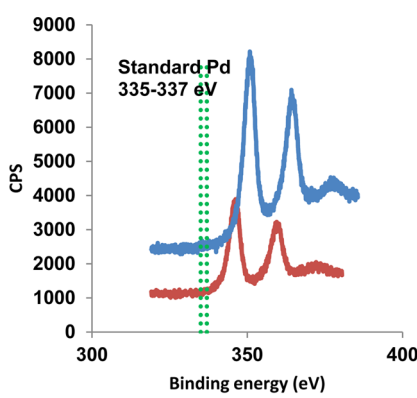


Figure 11. Pd 3d XPS of Pd–Cu/ZrO₂ catalyst.

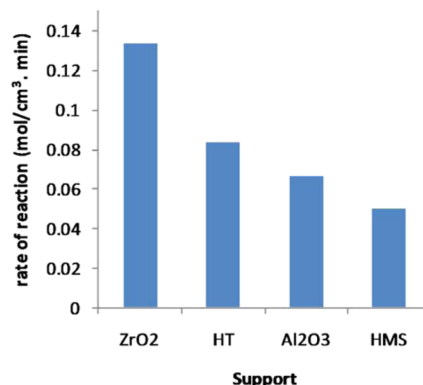


Figure 13. Comparison of the rate of LA hydrogenation reaction after 1 h of reaction with use of Pd–Cu active phase on ZrO₂, HT, Al₂O₃, and HMS as support.

(8) Desorption of PDO from acid site:



(9) Readsorption of PDO on acid site:



(10) Dehydration of PDO to form 2-MTHF:



(11) Desorption of 2-MTHF from acid site:



Table 5. Efficacy of Various Synthesized Catalysts on LA Hydrogenation^a

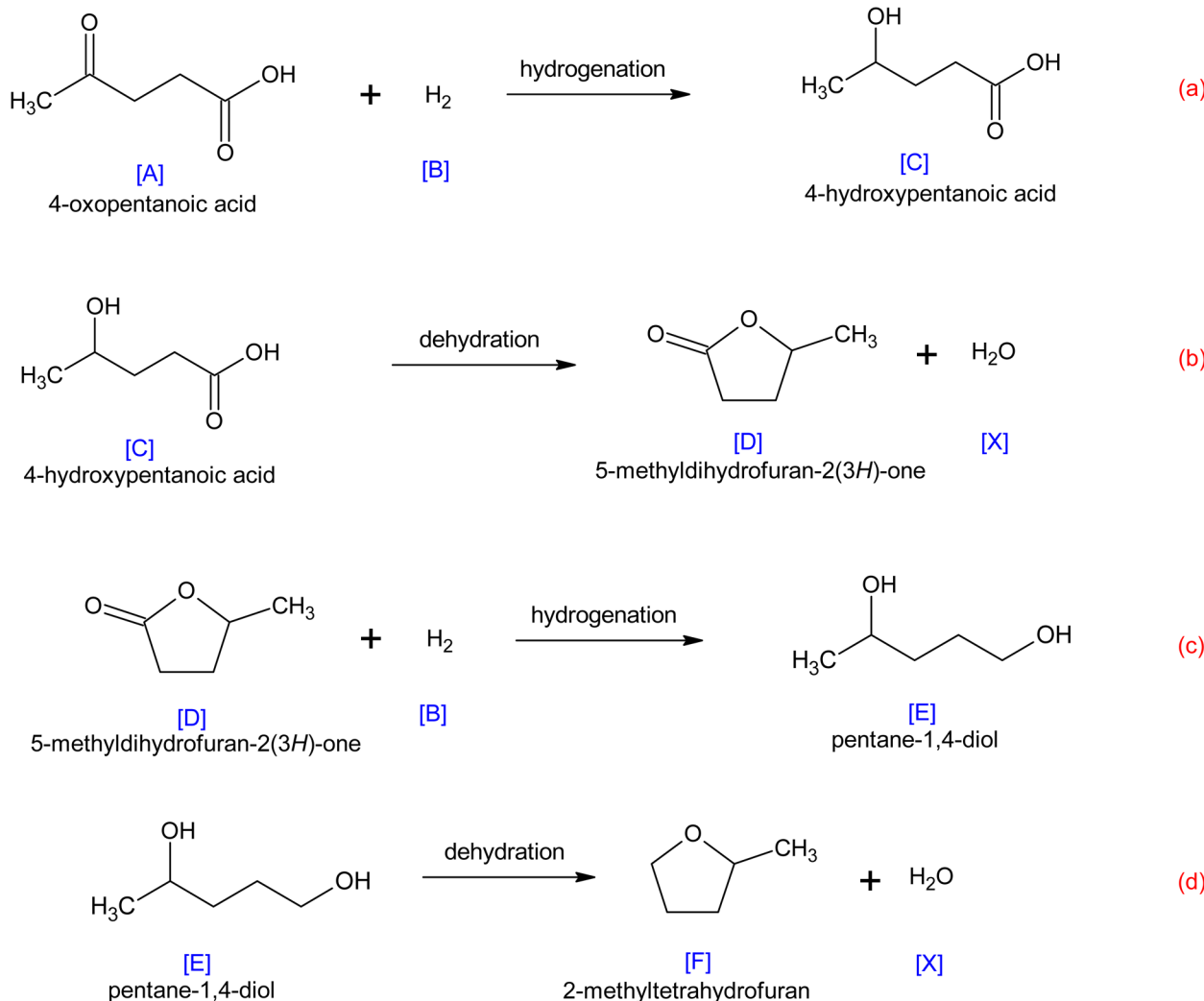
catalyst	conversion (%)	selectivity (%)		
		GVL	PDO	2-MTHF
Pd/ZrO ₂	marginal conversion (5%)			
Cu/ZrO ₂	100	70	25	5
Pd–Cu/ZrO ₂	100	70	25	5
Pd–Cu/HT	100	100	0	0
Pd–Cu/Al ₂ O ₃	100	100	0	0
Pd–Cu/HMS	100	100	0	0

^aLevulinic acid, 0.03 mol; water, 50 cm³; temperature, 200 °C; H₂ pressure, 60 atm; catalyst loading, 0.2 g/cm³; reaction time, 24 h.

Table 6. Atomic Absorption Spectroscopy Studies on Cu/ZrO₂ and Combinations of Pd–Cu/ZrO₂ Catalyst for Testing Leaching of Copper after Reuse

catalyst	initial rate of reaction (1 h reaction) (mol/cm ³ ·min)	selectivity (%) after 24 h			copper leaching (ppm)
		GVL	PDO	2-MTHF	
30%Cu/ZrO ₂	0.179	70	25	5	30.73
0.25%Pd–29.75%Cu/ZrO ₂	0.136	70	25	5	0.911
0.5%Pd–29.5%Cu/ZrO ₂	0.135	70	25	5	0.304
1%Pd–29%Cu/ZrO ₂	0.133	70	25	5	not detected

Scheme 1. Sequential Reactions to Yield 2-MTHF from LA Using Pd–Cu/ZrO₂ Catalyst



Considering the two hydrogenation steps of LA and GVL hydrogenation as slow steps, the net rate of hydrogenation can be expressed as

$$-r = k_1 C_A C_{B,S_m} + k_3 C_{D,S_a} C_{B,S_m} \quad (12)$$

$$-r = k_1 K_A C_A C_B C_{S_a} C_{S_m} + k_3 K_{D2} C_D C_B C_{S_a} C_{S_m} \quad (13)$$

$$C_{tm} = C_{B,S_m} + C_{S_m} \quad (14)$$

$$C_{tm} = \left[1 + K_A C_A + \frac{K_{D2} C_D C_X}{k_2} + K_{D2} C_D + K_{E2} C_E + K_F C_F \right] C_{S_m} \quad (15)$$

Substituting eqs 14 and 15 in eq 13

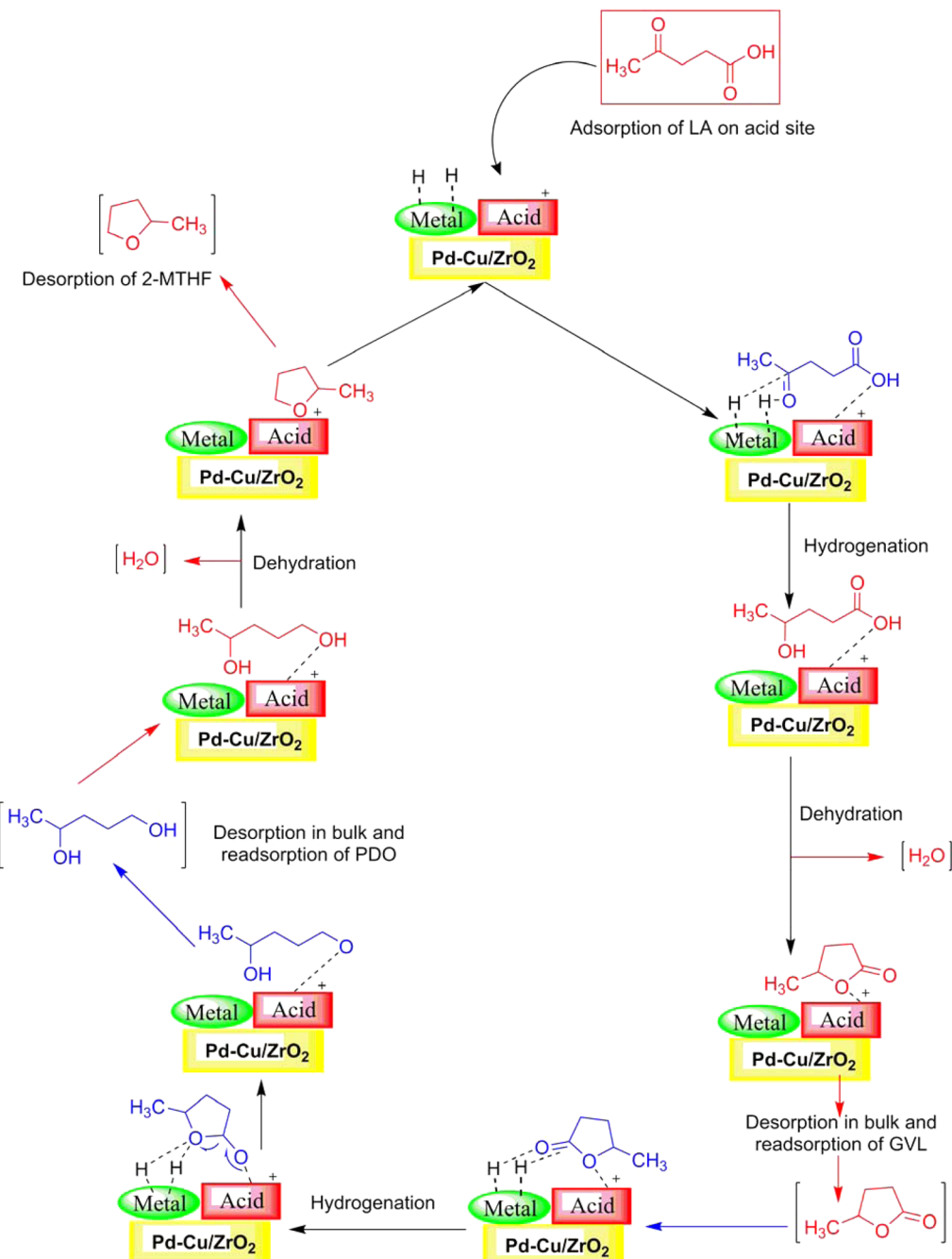
$$-r = \frac{[k_1 K_A C_A C_B + k_3 K_{D2} C_D C_B] C_{tm} C_{ta}}{\left[1 + K_A C_A + \frac{K_{D2} C_D C_X}{k_2} + K_{D2} C_D + K_{E2} C_E + K_F C_F \right] [1 + K_B C_B]} \quad (16)$$

$C_{tm} C_{ta} = kW$, where k is intrinsic kinetic constant and W is catalyst loading in g/cm³

$$-r = \frac{kW [k_1 K_A C_A C_B + k_3 K_{D2} C_D C_B]}{\left[1 + K_A C_A + \frac{K_{D2} C_D C_X}{k_2} + K_{D2} C_D + K_{E2} C_E + K_F C_F \right] [1 + K_B C_B]} \quad (17)$$

These steps are shown pictorially in Scheme 2.

To validate the mathematical equations derived for the rate of reaction, experiments were done after ensuring that there was no external mass transfer and pore diffusion resistances. It

Scheme 2. Mechanism of Synthesis of GVL, PDO, and 2-MTHF from LA on 1%Pd–29%Cu/ZrO₂ Catalyst

was observed that hydrogen pressure had no effect on the rate of reaction, and hence studies were done by varying catalyst loading and temperature only at constant hydrogen pressure. The reactions were carried out at different speeds of agitation from 800 to 1200 rpm. There was no effect on the rate of reaction by variation in rpm beyond 1000 rpm and hence it was concluded that there was no resistance due to external mass transfer. The Weisz-Prater moduli were calculated considering an average pore radius of 9 nm and particle radius of 25 μm . Tortuosity of 3 was assumed for the catalyst and diffusivity was calculated as $7 \times 10^{-8} \text{ m}^2/\text{s}$. Throughout the reaction, the values of the Weisz-Prater moduli remained far less than unity and hence it was concluded that reaction was intrinsically kinetically controlled. Experiments were done at different

catalyst loading from 0.1 to 0.3 g/cm³ (Figure 14). The initial rate of reaction increased with increase in the amount of catalyst. It indicated that the conversion was dependent on the active sites on the catalyst. The effect of temperature on the rate of reaction was studied by varying the temperature from 160 to 200 °C (Figure 15). The rate of reaction increased with the increase in temperature. The experimental data were used to find the reaction rate constants and adsorption constants numerically by interpolation. The values of adsorption and reaction rate constant were found to be consistent with temperature (Table 7). Arrhenius plot was made using the rate constant values for hydrogenation of LA and GVL. Activation energy for LA hydrogenation was found to be 16 kcal/mol and for GVL hydrogenation was found to be 21 kcal/mol (Figure

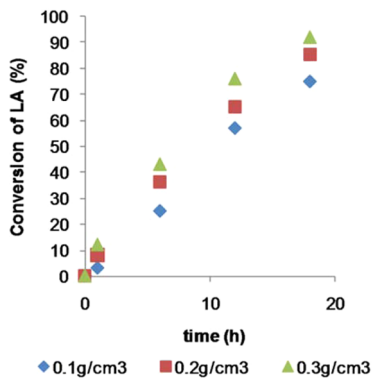


Figure 14. Effect of catalyst loading on the rate of LA hydrogenation reaction. Levulinic acid, 0.03 mol; water, 50 cm³; H₂ pressure, 60 atm; catalyst, Pd–Cu/ZrO₂; temperature, 200 °C; reaction time, 24 h.

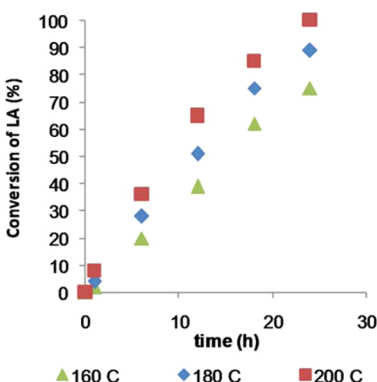


Figure 15. Effect of temperature on rate of LA hydrogenation reaction. Levulinic acid, 0.03 mol; water, 50 cm³; H₂ pressure, 60 atm; catalyst, Pd–Cu/ZrO₂; catalyst loading, 0.2 g/cm³; reaction time, 24 h.

16). The value of intrinsic kinetic constant was found to be 0.014 mol²·cm⁻³·g_{cat}⁻¹ (Figure 17). The reusability of the catalyst was checked by performing reactions with the same catalyst for 4 cycles. After each experiment, the catalyst was filtered out from the reactor and washed with water under reflux conditions at 100 °C. It was dried and used in the next cycle as is. The catalyst was found to be robust (Table 8). More pertinent stability studies were conducted by performing the reaction up to 18 h. The catalyst was then separated from reaction mixture. The same catalyst was then used with fresh reaction mixture. The catalyst performance was not hampered as it showed similar activity (Table 8). TPR data (Figure 3) indicate the presence of metal sites and the TPD-NH₃ data (Table 2) indicate presence of acid sites on Pd–Cu/ZrO₂ catalyst. The feasibility of the reaction itself indicates that the acid and metal sites are adjacent to each other. A parity plot (Figure 18) was plotted to validate the assumptions made during development of mathematical model. The identical values of theoretical and experimental rate of reaction indicate the assumptions made to derive the rate law are correct.

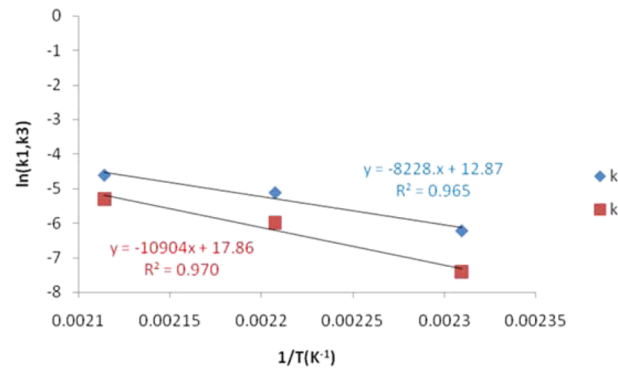


Figure 16. Arrhenius plot for calculating activation energy for LA hydrogenation and GVL hydrogenation.

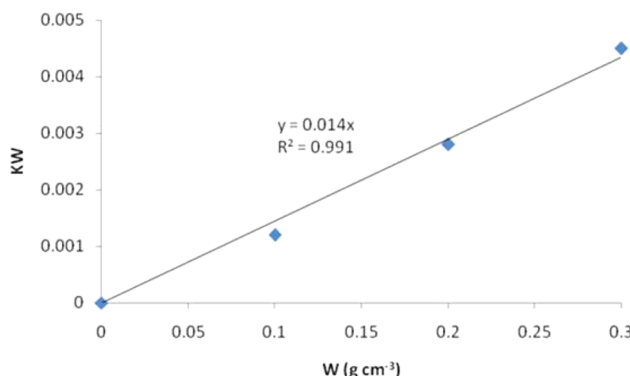


Figure 17. Plot to calculate intrinsic kinetic constant for cascade engineered LA hydrogenation.

Table 8. Conversion and Product Distribution with Fresh and Used Pd–Cu/ZrO₂ Catalyst

cycle	conversion (%) after 18 h	conversion (%) after 24 h	selectivity after 24 h		
			GVL	PDO	2-MTHF
0 (fresh catalyst)	85	100	70	25	5
1	85	100	70	25	5
2	80	100	75	22	3
3	75	100	80	19	1

CONCLUSION

The synthesis of GVL, PDO and 2-MTHF was achieved in a single pot starting from LA and hydrogen using 1% Pd–29% Cu/ZrO₂ catalyst and water as solvent at 200 °C and 60 atm H₂ pressure. The use of 30% Cu/ZrO₂ catalyst and water as solvent resulted in leaching of copper. The leaching was stopped completely by addition of palladium to Cu/ZrO₂ catalyst such that copper and palladium formed an alloy. The Pd–Cu/ZrO₂ catalyst was found to be robust and stable at high temperature and pressure although it reduced the initial rate of reaction marginally than the Cu/ZrO₂ catalyst. The effect of

Table 7. Values of Reaction Rate Constant and Adsorption Constants for One Pot Hydrogenation of Levulinic Acid

temp (°C)	k_1 (cm ³ ·mol ⁻¹ ·min ⁻¹)	k_3 (cm ³ ·mol ⁻¹ ·min ⁻¹)	K_A (cm ³ ·mol ⁻¹)	K_B (cm ³ ·mol ⁻¹)	K_{D2} (cm ³ ·mol ⁻¹)	$K_E \times 10^5$ (cm ³ ·mol ⁻¹)	$K_F \times 10^6$ (cm ³ ·mol ⁻¹)
160	0.002	0.0006	0.35	16.71	0.52	13.45	22.91
180	0.006	0.001	0.33	14.67	0.48	10.01	10.16
200	0.01	0.005	0.30	13.15	0.46	9.81	9.92

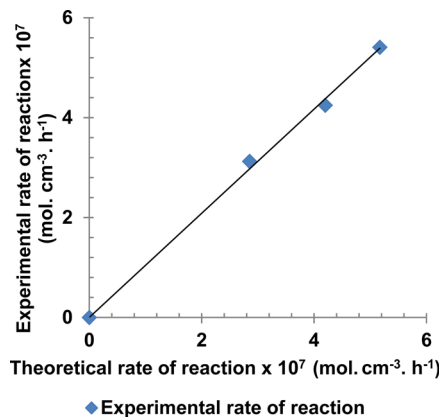


Figure 18. Parity plot to indicate validity of mathematical model for cascade engineered LA hydrogenation.

various supports was studied by making Pd–Cu/HT, Pd–Cu/Al₂O₃ and Pd–Cu/HMS catalysts. The reaction of LA hydrogenation using water as solvent was found to be sluggish using these catalysts. Hence even after 24 h of reaction, only GVL was obtained using these catalysts. The cascade engineered synthesis to yield PDO and 2-MTHF from LA occurred in 1% Pd–29% Cu/ZrO₂ catalyst because of larger pore size and acidity.

AUTHOR INFORMATION

Corresponding Author

*G. D. Yadav. E-mail: gd.yadav@ictmumbai.edu.in, gdyadav@yahoo.com. Tel.: +91-22-3361-1001. Fax: +91-22-3361-1020.

Notes

The authors declare no competing financial interest.

ACKNOWLEDGMENTS

S. C. Patankar acknowledges UGC for awarding SRF under its SAP programme (Centre of Advanced Studies in Chemical Engineering). G. D. Yadav acknowledges support from the R. T. Mody Distinguished Professor Endowment and J. C. Bose National Fellowship of Department of Science and Technology, Gov't. of India. The authors acknowledge the support provided by Indira Gandhi Centre for Atomic Research, Kalpakkam, India for the XPS characterization.

NOMENCLATURE

A = Levulinic acid

B = Hydrogen

C = Hydroxypentanoic acid

D = γ -Valerolactone

E = 1,4-Pantanediol

F = 2-Methyltetrahydrofuran

S_m = Metal site on the catalyst

S_a = Acid site on the catalyst

C_n ($n = A, B, C, D, E, F$) = Concentration of compound in bulk (mol/cm³)

C_{n,S_m} ($n = A, B, C, D, E$) = Concentration of compound on metal site (mol/cm³)

C_{n,S_a} ($n = C, D, E, F$) = Concentration of compound on acid site (mol/cm³)

K_A = Adsorption constant of levulinic acid on acid site (cm³.mol⁻¹)

K_B = Adsorption constant of hydrogen on metal site (cm³.mol⁻¹)

K_{C1} = Desorption constant of hydroxypentanoic acid from acid site (cm³.mol⁻¹)

K_{C2} = Adsorption constant of hydroxypentanoic acid on acid site (cm³.mol⁻¹)

K_{D1} = Desorption constant of γ -valerolactone from acid site (cm³.mol⁻¹)

K_{D2} = Adsorption constant of γ -valerolactone on acid site (cm³.mol⁻¹)

K_{E1} = Desorption constant of 1,4-pantanediol from acid site (cm³.mol⁻¹)

K_{E2} = Adsorption constant of 1,4-pantanediol on acid site (cm³.mol⁻¹)

K_F = Desorption constant of 2-methyltetrahydrofuran from acid site (cm³.mol⁻¹)

k_1 = Hydrogenation reaction rate constant for reaction of levulinic acid and hydrogen on metal site (cm³.mol⁻¹.min⁻¹)

k_2 = Reaction rate constant for dehydration reaction of hydroxypentanoic acid (min⁻¹)

k_3 = Hydrogenation reaction rate constant for reaction of γ -valerolactone and hydrogen on metal site (cm³.mol⁻¹.min⁻¹)

k_4 = Reaction rate constant for dehydration reaction of 1,4-pantanediol (min⁻¹)

REFERENCES

- Horvath, I. T.; Mehdi, H.; Fabos, V.; Boda, L.; Mika, L. γ -valerolactone- a sustainable liquid for energy and carbon based chemicals. *Green Chem.* **2008**, *10*, 238–242.
- (2) Final technical report: Commercialization of the BioFine technology for levulinic acid production from paper sludge; U.S. Department of Energy DOE/CE/41178; BioMeticsInc: Waltham, MA, 2002; www.osti.gov/scitech/servlets/purl/771246.
- (3) Mehdi, H.; Fabos, V.; Tuba, R.; Bodor, A.; Mika, L. T.; Horvath, I. T. Integration of homogeneous and heterogeneous catalytic processes for a multistep conversion of biomass: From sucrose to levulinic acid, γ -valerolactone, 1,4-pantanediol, 2-methyl-tetrahydrofuran, and alkanes. *Top. Catal.* **2008**, *48* (1), 49–54.
- (4) Christian, R. V.; Brown, H. D.; Hixon, R. M. Derivatives of γ -valerolactone, 1,4-pantanediol and 1,4-Di-(β -cynoethoxy)-pentane. *J. Am. Chem. Soc.* **1947**, *69*, 1961–1963.
- (5) Bourne, R. A.; Stevens, J. G.; Ke, J.; Poliakoff, M. Maximising opportunities in supercritical chemistry: the continuous conversion of levulinic acid to γ -valerolactone in CO₂. *Chem. Commun.* **2007**, 4632–4634.
- (6) Yan, Z. P.; Lin, L.; Liu, S. Synthesis of γ -valerolactone by hydrogenation of biomass derived levulinic acid over Ru/C catalyst. *Energy Fuels* **2009**, *23* (8), 3853–3858.
- (7) Upare, P. P.; Lee, J. M.; Hwang, D. W.; Halligudi, S. B.; Hwang, Y. K.; Chang, J. S. Selective hydrogenation of levulinic acid to γ -valerolactone over carbon supported noble metal catalysts. *J. Ind. Eng. Chem.* **2011**, *17* (2), 287–292.
- (8) Galletti, A. R.; Antonetti, C.; De Luise, V.; Martinelli, M. A sustainable process for the production of γ -valerolactone by hydrogenation of biomass derived levulinic acid. *Green Chem.* **2012**, *14*, 688–694.
- (9) Hengne, A. M.; Rode, C. V. Cu-ZrO₂ nanocomposite catalyst for selective hydrogenation of levulinic acid and its ester to γ -valerolactone. *Green Chem.* **2012**, *14*, 1064–1072.
- (10) Shimizu, K. I.; Kanno, S.; Kon, K. Hydrogenation of levulinic acid to γ -valerolactone by Ni and MoO_x co-loaded carbon catalysts. *Green Chem.* **2014**, *16*, 3899–3912.
- (11) Fu, S. Y.; Li, Y. Z.; Chu, W.; Li, C.; Tong, D. Monodisperse CuB₂₃ nanoparticles grown on grapheme as highly efficient catalysts for unactivated alkyl halide Heck coupling and hydrogenation. *Catal. Sci. Technol.* **2015**, *5*, 1638–1649.
- (12) Yan, K.; Liao, J.; Wu, X.; Xie, X. A noble metal free Cu catalyst derived from hydrotalcite for highly efficient hydrogenation of biomass derived furfural and levulinic acid. *RSC Adv.* **2013**, *3*, 3853–3856.

- (13) Climent, M. J.; Corma, A.; Iborra, S. Conversion of biomass platform molecules into fuel additives and liquid hydrocarbon fuels. *Green Chem.* **2014**, *16*, 516–547.
- (14) Yuan, J.; Li, S. S.; Yu, L.; Liu, Y. M.; Cao, Y.; He, H. Y.; Fan, K. N. Copper based catalysts for the efficient conversion of carbohydrate biomass into γ -valerolactone in the absence of externally added hydrogen. *Energy Environ. Sci.* **2013**, *6*, 3308–3318.
- (15) Li, M.; Li, G.; Li, N.; Wang, A.; Dong, W.; Wang, X.; Cong, Y. Aqueous phase hydrogenation of levulinic acid to 1,4-pentanediol. *Chem. Commun.* **2014**, *50*, 1414–1418.
- (16) Serrano-Ruiz, J. C.; Braden, D. J.; West, R. M.; Dumesic, J. A. Conversion of cellulose to hydrocarbon fuel by progressive removal of oxygen. *Appl. Catal., B* **2010**, *100* (1–2), 184–189.
- (17) Lange, J. P.; Price, R.; Ayoub, P. M.; Louis, J.; Petrus, L.; Clarke; Gosselink, H. Valeric biofuels: A platform of cellulosic transportation fuels. *Angew. Chem., Int. Ed.* **2010**, *49* (26), 4479–4483.
- (18) Bond, J. Q.; Alonso, D. M.; Wang, D.; west, R. M.; Dumesic, J. A. Integrated catalytic conversion of valerolactone to liquid alkenes for transportation fuels. *Science* **2010**, *327*, 1110–1114.
- (19) Du, X. L.; Bi, Q. Y.; Liu, Y. M.; Cao, Y.; He, H. Y.; Fan, K. N. Tunable copper-catalyzed chemoselective hydrogenolysis of biomass-derived γ -valerolactone into 1,4-pentanediol or 2-methyltetrahydrofuran. *Green Chem.* **2012**, *14*, 935–939.
- (20) Huber, G.; Iborra, S.; Corma, A. Synthesis of Transportation Fuels from Biomass: Chemistry, Catalysts, and Engineering. *Chem. Rev.* **2006**, *106*, 4044–4098.
- (21) Yadav, G. D. Insight into green phase transfer catalysis. *Top. Catal.* **2004**, *29* (3–4), 145–161.
- (22) (a) Yadav, G. D.; Patankar, S. C. Bimetallic heterogeneous catalyst for use in eco-friendly solvents. Ind. Patent 2511/MUM/2014, August 5, 2014. (b) Patankar, S. C.; Dodia, S. K.; Yadav, G. D. Cascade engineered synthesis of ethyl benzyl acetoacetate and methyl isobutyl ketone (MIBK) on novel multifunctional catalyst. *J. Mol. Catal. A: Chem.* **2015**, *409*, 171–182.
- (23) Wesche, R. *Physical Properties of High Temperature Superconductors*; John Wiley & Sons Ltd.: Chichester, U. K., 2015; pp 303, DOI: [10.1002/9781118696644](https://doi.org/10.1002/9781118696644).
- (24) Tanev, P. T.; Pinnavaia, T. J. A neutral templating route to mesoporous molecular sieves. *Science* **1995**, *267*, 865–867.
- (25) Macedo, M. Sol-gel synthesis of transparent alumina gel and pure gamma alumina by urea hydrolysis of aluminum nitrate. *J. Sol-Gel Sci. Technol.* **2004**, *30*, 135–140.
- (26) (a) Yadav, G. D.; Fernandes, G. P. Selective synthesis of natural benzaldehyde by hydrolysis of cinnamaldehyde using novel Hydro-talcite catalyst. *Catal. Today* **2013**, *207*, 162–169. (b) Doke, S. M.; Yadav, G. D. Synthesis of novel titania membrane support via combustion synthesis route and its application in decolorization of aqueous effluent using microfiltration. *Clean Technol. Environ. Policy* **2015**, DOI: [10.1007/s10098-015-1000-3](https://doi.org/10.1007/s10098-015-1000-3). (c) Yadav, G. D.; Gawade, B. A. Novelties of combustion synthesized and functionalised solid superacid catalysts in selective isomerisation of styrene oxide to 2-phenyl acetaldehyde. *Catal. Today* **2013**, *207*, 145–152. (d) Yadav, G. D.; Ajgaonkar, N. P.; Varma, A. Preparation of highly superacidic sulfated zirconia via combustion synthesis and its application in Pechmann condensation of resorcinol with ethyl acetoacetate. *J. Catal.* **2012**, *292*, 99–110. (e) Doke, S. M.; Yadav, G. D. Novelties of combustion synthesized titania ultrafiltration membrane in efficient removal of methylene blue dye from aqueous effluent. *Chemosphere* **2014**, *117*, 760–765.
- (27) Sengupta, D.; Saha, J.; De, G.; Basu, B. Pd/Cu bimetallic nanoparticles embedded in macroporous ion-exchange resins: an excellent heterogeneous catalyst for the Sonogashira reaction. *J. Mater. Chem. A* **2014**, *2*, 3986.
- (28) Addison, C. C.; Logan, N. Anhydrous metal nitrates. In *Advances in Inorganic Chemistry and Radiochemistry*; Emeleus, H. J., Sharpe, A. J., Eds.; Academic Press: New York, 1964.
- (29) Hinde, C. S.; Van Aswegen, S.; Holmes, J. D.; Hor, T. S.; Raja, R. Probing the design of in situ generated nanoparticles as sustainable oxidation catalysts. *Dalton Trans.* **2013**, *42*, 12600–12605.
- (30) Yuvaraj, S.; Yuan, L. F.; Huei, C. T.; Tih, Y. C. Thermal decomposition of metal nitrates in air and hydrogen environments. *J. Phys. Chem. B* **2003**, *107*, 1044–1047.
- (31) Carencio, S.; Hu, Y.; Florea, I.; Ersen, O.; Boissiere, C.; Sanchez, C.; Mezailes, N. Structural transitions at nanoscale: The example of palladium phosphides synthesized from white phosphorous. *Dalton Trans.* **2013**, *42*, 12667–12674.
- (32) Cusumano, J.; Dallabetta, R. A.; Levy, R. B. Multimetallic Catalysts. In *Catalysis in Coal Conversion*; Academic Press: London, 1978.
- (33) Sinfelt, J. H. Supported “bimetallic cluster” catalysts. *J. Catal.* **1973**, *29* (2), 308–313.
- (34) Boucher, M.; Zugic, G.; Cladaras, G.; Kammert, J.; Marcinkowski, M.; Lawton, T.; Skyes, C.; Stephanopoulos, M. Single atom alloy surface analogs in Pd0.18Cu15 nanoparticles for selective hydrogenation reactions. *Phys. Chem. Chem. Phys.* **2013**, *15*, 12187–12196.
- (35) Jin, X.; Dang, L.; Lohrman, J.; Subramaniam, B.; Ren, S.; Chaudhari, R. V. Lattice matched bimetallic CuPd-graphene nanocatalysts for facile conversion of biomass derived polyols to chemicals. *ACS Nano* **2013**, *7* (2), 1309–1316.